Research Article | Vol. 8, No. 2 | 1 Feb 2018 | OPTICAL MATERIALS EXPRESS 356
Optical Materials EXPRESS

Nonlinear optical response and structural properties of MBE-grown Fe:ZnS films

STANISLAV M. POLYAKOV,[1] ERIC KARHU,[1] REZA ZAMIRI,[2] CHARLES MOISSET,[3] KONSTANTINOS ILIOPOULOS,[3] PER ERIK VULLUM,[1,4] ULF L. OSTERBERG,[2,5] AND URSULA J. GIBSON[1,5,*]

[1]*Department of Physics, Norwegian University of Science and Technology (NTNU), N-7491 Trondheim, Norway*
[2]*Department of Electronic Systems, Norwegian University of Science and Technology (NTNU), N-7491 Trondheim, Norway*
[3] *Aix Marseille Univ, CNRS, Centrale Marseille, Institut Fresnel, Marseille, France*
[4]*Materials and Chemistry, SINTEF, NO-7465 Trondheim, Norway*
[5]*Department of Applied Physics, KTH Royal Institute of Technology, Stockholm, Sweden*
[*]*ursula.gibson@ntnu.no*

Abstract: Fe-doped ZnS films of high optical quality were fabricated using vacuum vapor deposition. Preferential crystalline orientation and phase purity of the host ZnS films were increased by the addition of small amounts of Fe, and the spectral shape of the 2-4 μm absorption peak is maintained up to the highest concentration tested (9 at.%). However, Raman shifts of the Fe:ZnS films indicate the inclusion of disordered material at high Fe concentrations, and below-gap optical Kerr effect measurements show an increase in $\chi^{(3)}$ correlated with this data. Nonlinear optical properties of the films were also measured using the Z-scan method at 532 nm, and saturable absorption of the Fe-based intraband levels at 2.94 μm was confirmed.

OCIS codes: (310.6860) Thin films, optical properties; (160.4670) Optical materials; (160.4330) Nonlinear optical materials.

References and links

1. R. E. Halsted and L. R. Koller, "Electroluminescence in Thin Films of ZnS:Mn," Phys. Rev. **93**, 349–350 (1954).
2. E. Malguth, A. Hoffmann, and M. R. Phillips, "Fe in III-V and II-VI semiconductors," Phys. Status Solidi (B) Basic Res. **245**, 455–480 (2008).
3. Y. Okada, N. J. Ekins-Daukes, T. Kita, R. Tamaki, M. Yoshida, A. Pusch, O. Hess, C. C. Phillips, D. J. Farrell, K. Yoshida, N. Ahsan, Y. Shoji, T. Sogabe, and J.-F. Guillemoles, "Intermediate band solar cells: Recent progress and future directions," Appl. Phys. Rev. **2**, 021302 (2015).
4. I. T. Sorokina and E. Sorokin, "Femtosecond Cr^{2+} - Based Lasers," IEEE J. Sel. Top. Quantum Electron. **21**, 2–4 (2015).
5. S. Mirov, V. Fedorov, I. Moskalev, M. Mirov, and D. Martyshkin, "Frontiers of mid-infrared lasers based on transition metal doped II-VI semiconductors," J. Lumin. **133**, 268–275 (2013).
6. I. S. Moskalev, V. V. Fedorov, and S. B. Mirov, "10-watt, pure continuous-wave, polycrystalline Cr^{2+}:ZnS laser." Opt. express **17**, 2048–2056 (2009).
7. E. A. Karhu, C. R. Ildstad, S. Poggio, V. Furtula, N. Tolstik, I. T. Sorokina, J. J. Belbruno, and U. J. Gibson, "Vapor deposited cr-doped zns thin films: towards optically pumped mid-infrared waveguide lasers," Opt. Mater. Express **6**, 2947–2955 (2016).
8. N. Tolstik, E. Sorokin, and I. T. Sorokina, "Ceramic Cr:ZnS Laser Mode-Locked by Graphene," Cleo: 2014 p. STu2E.7 (2014).
9. J. R. Macdonald, S. J. Beecher, A. Lancaster, P. A. Berry, K. L. Schepler, S. B. Mirov, and A. K. Kar, "Compact Cr:ZnS channel waveguide laser operating at 2333 nm," Opt. Express **22**, 7052–7057 (2014).
10. Y. P. Peng, X. Zou, Z. Y. Bai, Y. X. Leng, B. X. Jiang, X. W. Jiang, and L. Zhang, "Mid-infrared laser emission from Cr:ZnS channel waveguide fabricated by femtosecond laser helical writing," Sci. reports **5**, 18365 (2015).
11. E. Karhu, N. Tolstik, E. Sorokin, S. Polyakov, R. Zamiri, V. Furtula, U. Osterberg, I. T. Sorokina, and U. J. Gibson, "Towards Mid-IR Waveguide Lasers: Transition Metal Doped ZnS Thin Films," in "Conference on Lasers and Electro-Optics," (OSA, Washington, D.C., 2016), c, p. STu4R.2.
12. N. Tolstik, E. Sorokin, E. Karhu, S. Polyakov, U. Gibson, and I. T. Sorokina, "MBE-grown Cr:ZnS Thin Film Laser Media," in "Conference on Lasers and Electro-Optics," (OSA, Washington, D.C., 2016), p. JF1K.5.

#312915 https://doi.org/10.1364/OME.8.000356
Journal © 2018 Received 13 Nov 2017; revised 23 Dec 2017; accepted 9 Jan 2018; published 16 Jan 2018

Optical Materials EXPRESS

13. N. Tolstik, E. Sorokin, E. A. Karhu, K. Gorbachenya, S. M. Polyakov, V. Kisel, N. Kuleshov, I. T. Sorokina, and U. J. Gibson, "Spectral-luminescent properties of MBE-grown Cr:ZnS thin films and their application as saturable absorbers for 1.5-μm erbium lasers," (2016). In review.
14. N. Myoung, V. V. Fedorov, S. B. Mirov, and L. E. Wenger, "Temperature and concentration quenching of mid-IR photoluminescence in iron doped ZnSe and ZnS laser crystals," J. Lumin. **132**, 600–606 (2012).
15. L. D. DeLoach, R. H. Page, G. D. Wilke, S. A. Payne, and W. F. Krupke, "Transition metal-doped zinc chalcogenides: Spectroscopy and laser demonstration of a new class of gain media," IEEE J. Quantum Electron. **32**, 885–895 (1996).
16. V. I. Kozlovskii, Y. V. Korostelin, A. I. Landman, V. V. Mislavskii, Y. P. Podmar'kov, Y. K. Skasyrsky, and M. P. Frolov, "Pulsed Fe^{2+}:ZnS laser continuously tunable in the wavelength range of 3.49–4.65 μm," Quantum Electron. **41**, 1–3 (2011).
17. M. P. Frolov, Y. V. Korostelin, V. I. Kozlovsky, Y. P. Podmar'kov, S. a. Savinova, and Y. K. Skasyrsky, "3J pulsed Fe:ZnS laser tunable from 3.44 to 4.19μm," Laser Phys. Lett. **12**, 055001 (2015).
18. V. Fedorov, D. Martyshkin, M. Mirov, I. S. Moskalev, S. Vasilyev, J. Peppers, S. B. Mirov, and V. P. Gapontsev, "Fe-doped II-VI Mid-Infrared Laser Materials for the 3 to 8 μm Region," in "CLEO: 2013," (OSA, Washington, D.C., 2013), p. JM4K.2.
19. K. N. Firsov, E. M. Gavrishchuk, V. B. Ikonnikov, S. Y. Kazantsev, I. G. Kononov, S. A. Rodin, D. V. Savin, and N. A. Timofeeva, "High-energy room-temperature Fe^{2+}:ZnS laser," Laser Phys. Lett. **13**, 015001 (2016).
20. A. Martines, A. A. Gallian, P. Marine, V. Fedorov, S. Mirev, V. Badikov, and A. Martinez, "Fe:ZnSe and ZnS Polycrystalline Passive Q-Switching of 2.8 μm Er:Cr:YSGG Laser," Adv. Solid-State Photonics (ASSP) pp. 40–42 (2007).
21. S. B. Mirov, "Saturable absorbers for Q-switching of middle infrared laser cavaties," (2008).
22. N.-A. Molland, Z. Ghadyani, E. a. Karhu, S. Poggio, M. Nematollahi, M. Kildemo, T. W. Reenaas, J. J. BelBruno, and U. J. Gibson, "Band-edge modification and mid-infrared absorption of co-deposited $Fe_xZn_{1-x}S$ thin films," Opt. Mater. Express **5**, 1613 (2015).
23. Q. J. Feng, D. Z. Shen, J. Y. Zhang, Y. M. Lu, Y. C. Liu, and X. W. Fan, "Influence of Fe content on the structural and optical properties of ZnFeS thin films," Mater. Chem. Phys. **96**, 158–162 (2006).
24. F. Zhu, S. Dong, and G. Yang, "Ferromagnetic properties in Fe-doped ZnS thin films," Optoelectronics Adv. Materials, Rapid Commun. **4**, 2072–2075 (2010).
25. R. Swanepoel, "Determination of the thickness and optical constants of amorphous silicon," J. Phys. E: Sci. Instruments **16**, 1214–1222 (1983).
26. S. J. Byrnes, "Multilayer optical calculations," ArXiv e-prints (2016).
27. P. P. Ho and R. R. Alfano, "Optical kerr effect in liquids," Phys. Rev. A **20**, 2170–2187 (1979).
28. J. E. Aber, M. C. Newstein, and B. A. Garetz, "Femtosecond optical kerr effect measurements in silicate glasses," J. Opt. Soc. Am. B **17**, 120–127 (2000).
29. M. Sheik-Bahae, A. A. Said, T. H. Wei, D. J. Hagan, and E. W. V. Stryland, "Sensitive measurement of optical nonlinearities using a single beam," IEEE J. Quantum Electron. **26**, 760–769 (1990).
30. K. Iliopoulos, A. El-Ghayoury, H. E. Ouazzani, M. Pranaitis, E. Belhadj, E. Ripaud, M. Mazari, M. Sallé, D. Gindre, and B. Sahraoui, "Nonlinear absorption reversing between an electroactive ligand and its metal complexes," Opt. Express **20**, 25311–25316 (2012).
31. T. Olivier, F. Billard, and H. Akhouayri, "Nanosecond z-scan measurements of the nonlinear refractive index of fused silica," Opt. Express **12**, 1377–1382 (2004).
32. W. G. Nilsen, "Raman spectrum of cubic ZnS," Phys. Rev. **182**, 838–850 (1969).
33. Y. C. Cheng, C. Q. Jin, F. Gao, X. L. Wu, W. Zhong, S. H. Li, and P. K. Chu, "Raman scattering study of zinc blende and wurtzite ZnS," J. Appl. Phys. **106**, 123505 (2009).
34. O. Brafman and S. S. Mitra, "Raman effect in wurtzite- and zinc-blende-type ZnS single crystals," Phys. Rev. **171**, 931–934 (1968).
35. S. Jiménez-Sandoval, A. López-Rivera, and J. C. Irwin, "Influence of reduced mass differences on the Raman spectra of ternary mixed compounds: $Zn_{1-x}Fe_xS$ and $Zn_{1-x}Mn_xS$," Phys. Rev. B **68**, 054303 (2003).
36. W. Giriat and J. K. Furdyna, *Semiconductors and semimetals* (Academic Press Inc., 1988), vol. 25, chap. 1.
37. M. Zigone, M. Vandevyver, and D. N. Talwar, "Raman scattering and local force variations due to transition-element impurities in zinc-sulfide crystals: Effect of pressure application," Phys. Rev. B **24**, 5763–5778 (1981).
38. D. L. Peterson, A. Petrou, W. Giriat, A. K. Ramdas, and S. Rodriguez, "Raman scattering from the vibrational modes in $Zn_{1-x}Mn_xTe$," Phys. Rev. B **33**, 1160–1165 (1986).
39. S. Wang, Y. Zhang, J. Xing, X. Liu, H. Yu, A. DiLieto, M. Tonelli, T. Sum, H. Zhang, and Q. Xiong, "Nonlinear optical response of Au nanorods for broadband pulse modulation in bulk visible lasers," Appl. Phys. Lett. **107**, 161103–1–161103–5 (2015).
40. M. Haiml, R. Grange, and U. Keller, "Optical characterization of semiconductor saturable absorbers," Appl. Phys. B **79**, 331–339 (2004).
41. Y. Wang, P. Thomas, and P. O'Brien, "Optical properties of ZnO nanocrystals doped with Cd, Mg, Mn, and Fe ions," J. Phys. Chem. B Lett. **110**, 21412–21415 (2006).
42. V. V. F. S. B. M. J. Peppers, D. V. Martyshkin, "Spectroscopic characterization and energy transfer process in cobalt and cobalt-iron co-doped ZnSe/ZnS crystals," ProcSPIE **8959**, 8959 – 8959 – 7 (2014).
43. A. L. Patterson, "The scherrer formula for x-ray particle size determination," Phys. Rev. **56**, 978–982 (1939).

Optical Materials EXPRESS

1. Introduction

Transition metal substitution in II-VI semiconductors has been a rich area of study for over 50 years [1] but new applications, including dilute magnetic semiconducting devices [2], intermediate band solar cells [3], and mid-infrared lasers [4, 5] are driving further development of these materials. In particular, both ZnS and ZnSe have suitable properties as hosts for passive Q-switch and gain species in the mid-infrared region. In general, ZnS exhibits superior thermal properties [6]. The most promising dopants are Cr^{2+} and Fe^{2+} due to their well-isolated transitions within the semiconductor bandgap. Cr^{2+} doped films of high quality have recently been introduced [7] and Fe^{2+} doped thin films represent a technologically important extension of these results,as they extend the accessible wavelength range of miniature devices. Fluorescence efficiency, carrier lifetimes and concentration quenching are critical for lasing, while in the case of saturable absorbers, Kerr lensing and nonlinear absorption are key properties.

Recently, significant progress has been made with Cr in Zn(S,Se) single crystal, polycrystalline ceramic and thin film hosts. Cr^{2+} doped ceramic ZnS has been successfully used for lasers in the 2–4 μm band [8]. Initially, confinement was provided by using femtosecond processing to define the boundaries of a waveguide [9, 10] within a bulk sample, but new studies [11, 12] suggest that vacuum-deposited thin films may be suitable for fabrication of waveguide or disk lasers. Moreover, MBE-grown Cr:ZnS thin films show promise as saturable absorbers for 1.5 μm erbium lasers [13].

There is significant interest in Fe doped Zn(S,Se) systems, as gain and saturable absorber materials [14, 15], and both crystals and ceramic forms are commercially available. Recent work on Fe:ZnS has demonstrated lasing in the 3–5 μm wavelength region with Er:YAG and HF pump lasers [16–19], including operation at room temperature. Single crystals are difficult to fabricate, and polycrystalline hot pressed ceramics are an alternative suitable for use as Q-switches [20, 21]. To date, doping has been performed either during crystallization, or post-growth into single crystal or polycrystalline samples. In the latter process, a thin film of the metal is deposited onto the sample surface, and a high temperature annealing allows diffusion of the dopant into the bulk. This process typically results in a rapidly varying concentration profile near the surface [14].

Fe:ZnS thin films have received less attention [22–24], but an isolated absorption (Fe^{2+}) peak was observed at concentrations as high as 2 at.% Fe - much higher than the level where a well-defined peak is observed for Cr^{2+} doped ZnS [11]. This observaton, combined with results on Cr-doped films, suggests that vapor deposition of Fe:ZnS may be a route to a fabrication of thin film saturable absorbers for passive Q-switches at longer wavelengths. Thin film devices offer compactness and the advantage that the dopant profile can be controlled during the deposition and concentrations beyond the bulk solubility are possible. However, high concentrations are only useful if the Fe is substitutional, and the underlying crystal structure is not degraded unduly by its introduction. Early results on Fe- substituted ZnS films suggested that these requirements were met, even with readily accessible vacuum levels. In order to establish the potential of the thin-film materials, we have made detailed studies of the relationship between the optical properties and the structure in films with up to 9 at.% Fe in ZnS. We present Raman and x-ray diffraction results, direct imaging of the film structure by transmission electron microscopy (TEM), and results on the nonlinear optical properties of the materials in several regimes.

2. Experimental

A series of films, 3-5 μm in thickness, with different amounts of Fe, were deposited in an ultrahigh vacuum (UHV) chamber with a base pressure of 5×10^{-7} Pa. Fe (99.98%, Sigma Aldrich) was e-beam evaporated, while ZnS (99.99%, Alfa Aesar) was evaporated from a Knudsen cell. Although high vacuum levels were acheivable, the primary advantage of this deposition system was the well-controlled deposition rates, assuring uniform doping. Single crystal (100)

Optical Materials EXPRESS

silicon (1 cm × 1 cm) and c-plane sapphire (1 cm diameter) were used as substrates to minimize background signals during analysis, rather than to promote epitaxial growth. Before loading, the substrates were sequentially cleaned in ultrasound baths of acetone and isopropanol and blown dry with nitrogen. The deposition rate for Fe was varied between 0.14 Å/s and 0.30 Å/s, and for ZnS, a rate between 3.11 Å/s and 7.45 Å/s was used. Substrates were held at room temperature (RT) in a rotating sample holder. The physical thicknesses were confirmed using Veeco Dektak 150 profilometer and elemental composition of the films was investigated with an energy-dispersive X-ray spectroscopy (EDS) system of Hitachi TM3000 scanning electron microscope.

Optical properties were assessed using linear and Raman spectrometry, Optical Kerr Effect (OKE) and intensity-dependent laser transmission measurements. The pulses used are very different at the different wavelengths for these preliminary results, but we are able to demonstrate non-linear behavior over a wide spectral and temporal range. Spectral transmission information was determined at room temperature with a double-beam UV/VIS/NIR spectrophotometer (OLIS 14, On-line Instrument Systems, Inc.) in the wavelength range 340 to 2600 nm. Fourier transform infrared spectroscopy (FTIR) in transmission mode was carried out at room temperature (RT) and at cryogenic temperatures with Bruker Vertex and ISF 125 HR Bruker Optic spectrometers respectively. To extract index, absorption and thickness of the films, an analysis based on Swanepoel et al. [25] was performed on the room temperature optical data. Due to the more detailed structure in the data at low temperatures, modeling was also performed with an iterative fitting procedure to get the best match to the observed spectrum, using a transfer matrix method (TMM) to calculate the transmission [26]. Nonlinear optical properties were assessed in several regimes. Optical Kerr effect properties of the films were measured in a standard configuration at 795 nm, and non-linear effects were probed using both an Er:YAG laser at 2940 nm, and a doubled YAG laser at 532 nm.

Optical Kerr Effect experiments [27, 28] were carried out using a Kerr lens mode-locked Ti:Sapphire oscillator and a chirped pulse amplification system. The (λ=795 nm) pulses, far enough from any resonance that the results should be representative for most energies, were 70 fs long and had a 1 kHz repetition rate. Saturable absorption was measured using an Er:YAG laser at 2.94μm (0.42 eV) with a pulse length of 100 μs and a repetition rate of 5Hz. The pulse energy was 200 mJ, the peak power was 2kW and the beam radius was 1.7mm at the laser aperture and approx. 200μm at the focus. The wavelength was chosen because it is within the linewidth of the $^5E \rightarrow {}^5T_2$ transition for Fe^{2+} ions. The intensity was varied by moving the sample along the Gaussian beam trajectory created by a lens with focal length of 50mm.

Z-scan measurements [29–31] were performed using 11 ns laser pulses at 532 nm with a 10Hz repetition rate to determine separately the nonlinear refraction and the nonlinear absorption of the samples, related to the real and imaginary parts of the third order nonlinear susceptibilities, respectively ($\mathrm{Re}\chi^{(3)}$, $\mathrm{Im}\chi^{(3)}$). At this wavelength, the linear absorption due to imperfections is approximately a factor of two higher than at the wavelength used for OKE studies. Special care was taken to assure that no permanent modification of the samples took place during the measurements.

Structural properties were examined by X-ray diffraction (XRD) and transmission electron microscopy (TEM). The crystallographic data of the films on Si substrates were collected in θ-2θ configuration using Bruker diffractometer with a monochromator (λ = 0.15418 nm). The cross-section TEM sample was prepared by a FEI Helios Nanolab dual-beam FIB. Prior to FIB sample preparation, a 25 nm thick layer of Au was sputter coated on top of the wafer. To protect the region of interest from Ga ion-beam damage, e-beam assisted deposition of a thin Pt layer (ca. 100 nm) followed by ion-beam assisted deposition of a 2 μm thick C layer were coated on top of the Au layer. The coarse Ga^+ ion-beam thinning was done at 30 kV acceleration voltage followed by final thinning at 5 kV. TEM was performed with a double Cs corrected cold FEG

Optical Materials EXPRESS

JEOL ARM200CF, operated at 200 kV.

3. Results and discussion

3.1. FTIR

The absorption coefficients for different concentrations of Fe in ZnS were extracted by Swanepoel [25] analysis and iterative fitting using transfer matrix method (TMM) [26]. A comparison of these methods for RT measurements is shown in Fig. 1 (a). The absorption peak at 2.8 μm, associated with Fe substitution on Zn lattice sites, remains well isolated, with little visible absorption, for concentrations up to 4 at.%, in a good agreement with the DFT calculations [22] reported by Molland et al. and similar to previous experimental results on bulk crystals [20]. Above 4 at.%, the intraband Fe levels retain their structure, but the short-wavelength absorption increases, either due to a reduction in the bandgap of the alloyed ZnS, or due to non-substitutional Fe - either in clusters or at grain boundaries. Although the Swanepoel analysis inherently masks fine structure (due to the exclusive use of the transmission extrema), little structure within the absorption peak is expected at RT due to thermal smearing. Results of both modeling techniques are shown for comparison. The high frequency oscillations in the calculated spectra are indicative of an imperfect fit to the index of refraction of the film.

Low temperature (35 K) spectra for the samples with the isolated Fe peaks are presented in Fig. 1 (b) together with a single crystal absorption curve [17] measured by Frolov et al. at 77 K; temperature-depended measurements are shown in Fig. 1 (c). According to crystal field theory, the ^{5}D state is split into ^{5}E ground and $^5T_2$ excited states, which in case of tetrahedral Fe^{2+} have 5 and 6 spin-orbit levels respectively. The $^5E \rightarrow {}^5T_2$ transitions are allowed and for Fe:ZnS system we expect to see multiple absorption lines between ≈ 2000 nm and ≈ 4000 nm. $\Gamma_5(^5T_2) \rightarrow \Gamma_1(^5E)$ transition energy was reported to be equal to 365.5 meV [2] and is thought to be responsible for the 3396 nm peak in the absorption spectra. A satellite peak at lower energies around 3549 nm, can be explained by a phonon assisted transition or by the defects in the cubic/hexagonal polycrystalline films. It is remarkable that the structure of the absorption spectrum is retained at 1.2 at.% with good fidelity, and is little changed even for 7 at.% Fe.

3.2. Optical Kerr effect

The third-order nonlinearity term $\chi^{(3)}$ is a direct indication of the potential of a material for Kerr lensing effects, which would enhance saturable absorption. Preliminary measurements of the OKE response were made at 795 nm (the Kerr effect behavior should be similar for other wavelengths in the absence of resonances). Linear absorption was significant at this wavelength for the highest concentrations, and may be associated with non-substitutional Fe, as discussed above.The results in Fig. 1 (d) are for 2 mW average input power, below the onset of nonlinear absorption.

The value of the $\chi^{(3)}$ of the films were calculated from the OKE signals using the following equation:

$$\chi_s^{(3)} = \chi_r^{(3)} \times \left(\frac{I_s}{I_r}\right)^{\frac{1}{2}} \times \left(\frac{n_s}{n_r}\right)^2 \times \left(\frac{L_r}{L_s}\right) \times \frac{\alpha L_s}{\exp(-\frac{\alpha L_s}{2}) \times [1 - \exp(-\alpha L_s)]}, \quad (1)$$

where I is the intensity of the OKE signal at zero delay time, α is the linear absorption coefficient of the sample, n is the refractive index, and L is the interaction length of probe and pump beam in the sample. The subscripts s and r denote sample and reference, respectively. Here, we used sapphire substrate as a reference sample with a known value of $\chi^{(3)} \sim 2.2 \times 10^{-14}$esu. A pure ZnS film has $\chi^{(3)} \sim 4.2 \times 10^{-11}$ esu. Little change is seen until the concentration of Fe reaches ~ 7 at.%, where there is a sharp increase to 17.5×10^{-11} esu. This correlates with where the Raman results show that significant structural changes are introduced in the ZnS by the presence

Optical Materials EXPRESS

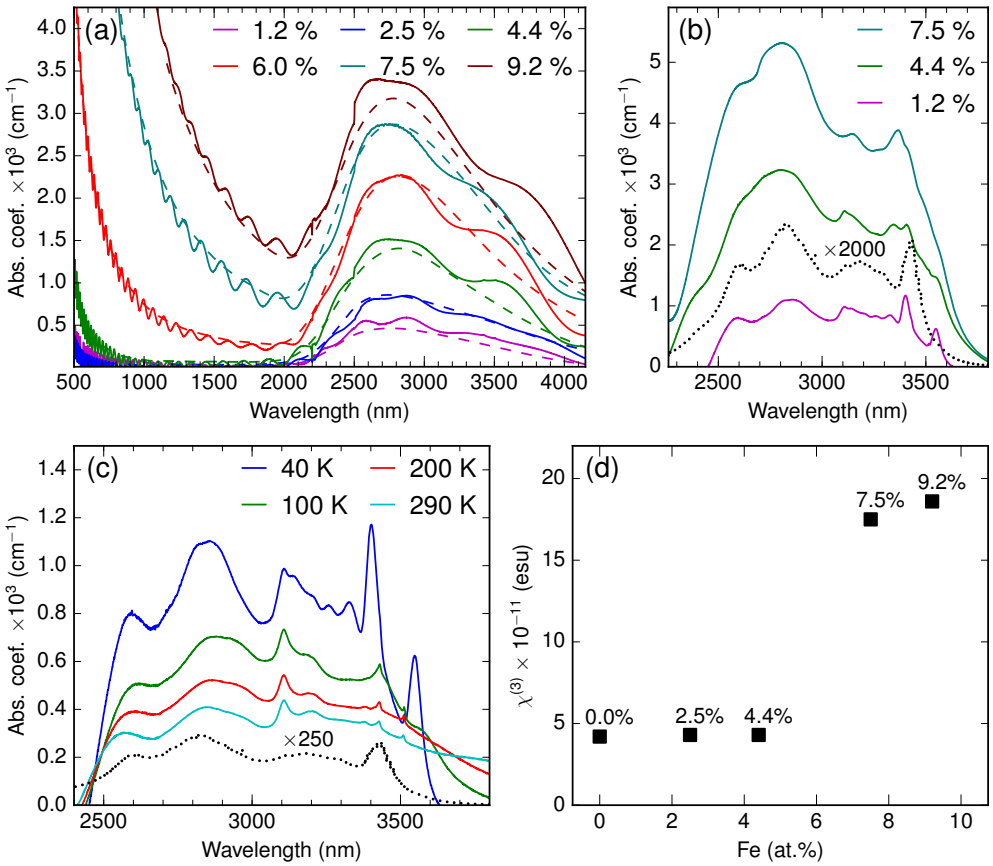

Fig. 1. (a) Room temperature measurements, Absorption coefficient (α) of Fe:ZnS films with different Fe concentrations extracted from transmission data using Swanepoel (dashed line) and TMM (solid line) modeling methods. (b) Absorption coefficient (TMM) at 35K, and a reference single crystal (concentration 0.01%) spectrum (dotted lines) [17] taken at 77 K. (c) Temperature dependence of the absorption coefficient (TMM) for a 1.2 at.% Fe:ZnS sample. The small peak at 3100 nm is due to a thin ice film deposited on the surface in the cryostat. (d) $\chi^{(3)}$ as a function of Fe content from OKE measurements at 795 nm.

of Fe. The temporal response of the OKE signal was insensitive to the inclusion of Fe, even at high concentrations, when measured in the low power regime.

3.3. Raman

Raman spectroscopy provides insight into the structural order by probing the vibrational modes in the material directly. Measurements were made of both the first and second-order peaks to look for the onset of disorder in the films.

Fig. 2 shows the Raman spectra acquired at RT from ZnS films with different amount of doping. Raman modes of both cubic zincblende (ZB) and hexagonal wurtzite (W) ZnS are well studied. It is reported that first-order transverse optical (TO) phonons in both of the polymorphs and similarly longitudinal optical (LO) phonons are very close in frequency [32–34]. As can be seen in Fig. 2 (a), for pure ZnS, only one peak was observed at 351 cm^{-1} and it can be assigned to either $A_1(LO)$, $E_1(LO)$ modes in W and LO in ZB [34]. None of the TO phonons expected

Optical Materials EXPRESS

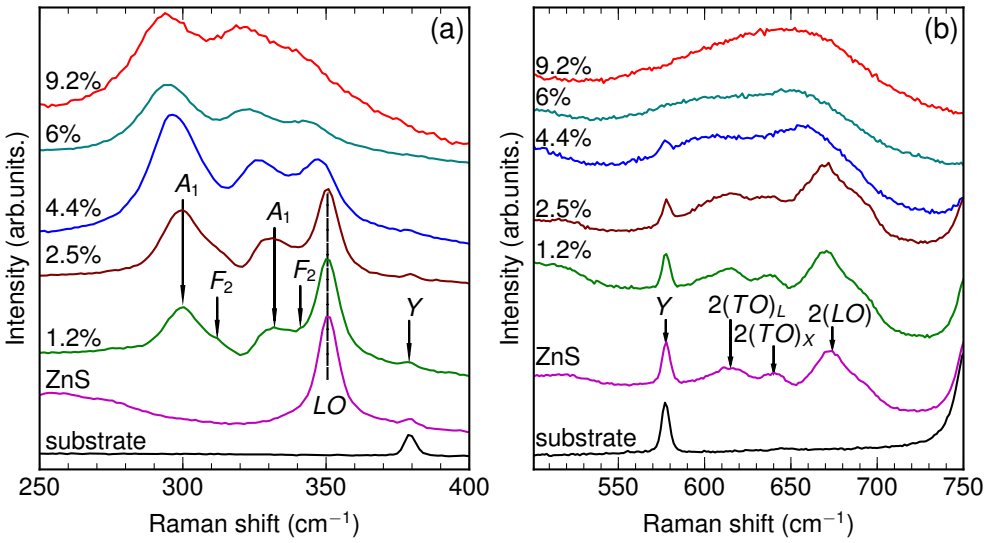

Fig. 2. Room-temperature Raman spectra of Fe:ZnS for different Fe concentrations. The sapphire substrate vibrational peaks are indicated as Y and the ZnS modes are described in the text, including vibrational modes of A_1, and F_2 type symmetries, denoted here as A_1 and F_2. (a) First-order peaks; (b) Second-order peaks.

around 275 cm^{-1} were clearly observed in our spectra, which is generally accepted as LO modes dominate over the TO ones [32]. To distinguish between the two ZnS crystal structures we studied the second-order Raman spectra, which are depicted in Fig. 2 (b). The three lines that appear at 615, 640 and 673 cm^{-1} can be identified as $2(TO)$, $2(LO)$ processes at different Brillouin zone points. These values are in a good agreement with previously published results for cubic ZB ZnS [32, 33]. With increasing Fe content we can see that the cubic structure is preserved, but the peaks shift because the lattice parameter is changing. Higher disorder results in a broadening of the peaks, which corresponds with the previous observations of $Fe_xZn_{1-x}S$ crystals with $x > 0.05$ [35, 36]. In theory, a perfect diatomic crystal is transparent to IR radiation between the $(TO)_\Gamma$ and $(LO)_\Gamma$ frequencies, but substitutional impurities in ZB crystal are expected to appear as vibrational modes of the A_1, and F_2 type symmetries in between TO and LO positions [35, 37]. Fig. 2 (a) shows the appearance of all four modes with A_1 type vibrations dominating, and confirms the substitutional Fe incorporation. With the increasing concentration of Fe, we can observe the shift of the peaks to lower frequencies in contrast to the previously reported results [35], but similar to another zinc chalcogenide $Zn_{1-x}Mn_xTe$ [38]. Good structural order is indicated for films up to 4% Fe content.

3.4. Nonlinear optical response

Nonlinear absorption: Transmission results at 2.94 μm for two different samples (2 and 5.8% Fe, thicknesses 4.5 and 3.3μm respectively) are shown in Fig. 3. Possible contributions from the sapphire substrate were excluded. While the shape of the visible spectrum for films with more than 4% Fe changes appreciably from those with less, the spectral shape of the infrared absorption peak does not, and the non-linear transmission did not change markedly above and below this threshold.

For the film with 5.8 at.% Fe^{2+} (inset) the saturable absorption I_{sat} was modeled to be ~ 1.79

Optical Materials EXPRESS

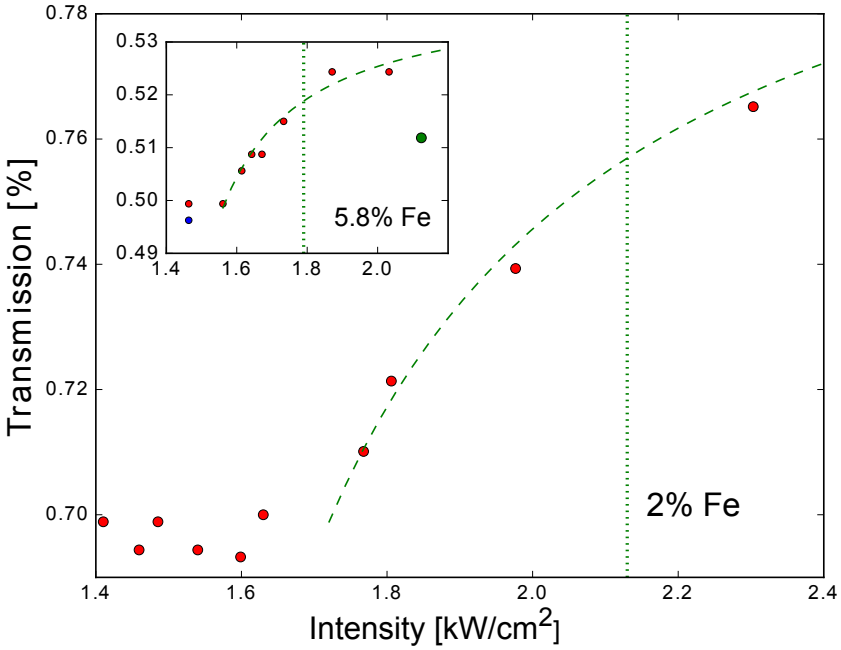

Fig. 3. a) Nonlinear transmission of Fe-doped ZnS film with 2% Fe at 2.94μm . Inset is for film with 5.8% Fe. Vertical dotted lines indicate the saturable intensity I_{sat}.

kW/cm^2 with a transmission modulation ΔT of 3.5% while for the film with 2 at% Fe^{2+} I_{sat} was 1.95 kW/cm^2 and the transmission modulation was 8%. The analysis was based on a two-level model for the iron $^5E \rightarrow {}^5T_2$ transition within the bandgap resulting in the power dependent formula for the nonlinear part of the transmission curve [39]:

$$T = A \exp[-\Delta T/(1 + I/I_{sat})] \tag{2}$$

The sample with fewer Fe ions had a higher saturation intensity, I_{sat}, as expected from a two-level system. The measurements in the saturated regime did not show evidence of other nonlinear interactions such as two-photon absorption or excited-state absorption [40].

With long pulses ($\mu s \rightarrow ms$) there is always a concern that thermal effects may contribute to the nonlinear absorption. Thermal nonlinear absorption has been reported in ZnS films but only for wavelengths in the blue, close to the bandgap, while the laser photon energy used here was 0.42 eV and the ZnS bandgap is 3.7 eV. Nevertheless, we performed measurements on a pure ZnS film and no saturable absorption was observed. Thermal effects are not expected to play a role in nonlinear absorption at this wavelength for the iron-doped samples since the energy levels are well within the bandgap and absorption to conduction band states is forbidden by transition rules [41].

Increasing transmission was seen with increasing intensity despite the long pulse length (nominally 100 μs). For both films, the non-linear behavior was preceded at low intensities by an approximately constant transmission region.The absorption values of the films are at least 50-75 times higher than commercially available Fe:ZnS materials, which makes it difficult to extrapolate the non-linear behavior. The measurements are also made with long pulses compared to most studies, which is likely responsible for the observed low damage threshold, and possibly leading to the small I_{sat} values. The two films are expected to have different properties because they lie on opposite sides of the 4% threshold where the linear absorption properties change

Optical Materials EXPRESS

significantly, either due to defects or band gap modification, but both clearly show saturable absorption below the damage threshold.

The green marker in the inset of Fig. 3 shows the transmission value after the film had been optically damaged. The film with less iron had a higher damage threshold, of around 3 kW/cm^2. Possible factors in the observed damage thresholds are stresses due to grain-boundaries, the long pulse lengths, and the fact that not all Fe^{2+} ions are substitutional in the ZnS lattice at these high concentrations.

Z-scan measurements: While OKE measurements can detect refractive index modifications, Z-scan can investigate many mechanisms including thermal effects. The difference in wavelength between the sources and the broader sensitivity of Z-scan make these measurements an interesting supplement to the OKE results. Z-scan measurements on a 3.3 μm thick film with a 5.8% Fe content were performed at 532 nm, using 11 ns pulses by simultaneously measuring the transmission after the sample in two different ways. By detecting either the total laser beam ('open-aperture' Z-scan) or a part of the laser beam passing through a pinhole ('closed-aperture' Z-scan). The open-aperture Z-scan allowed the determination of the nonlinear absorption of the samples. The division of the closed-aperture by the open-aperture curves allowed the determination of the nonlinear refraction by eliminating the nonlinear absorption contribution to the nonlinear optical response ('divided' Z-scan). The advantage of the Z-scan technique is that it can provide the magnitude as well as the sign of the nonlinearity.

Several Z-scans were recorded at different laser energies in order to find the range which gave a significant signal to noise ratio without permanent damage of the material. This energy range was found to be between 1.0 μJ and 3.5 μJ per pulse. Examples of both divided and open aperture Z-scans can be seen in Fig. 4. The divided Z-scans have a valley-peak configuration revealing that the sample exhibits self-focusing (positive nonlinear refractive index). A transmission valley in the case of the open-aperture Z-scan indicates a reverse saturable absorption(RSA)-type behaviour (positive nonlinear absorption parameters) at this wavelength.

The experimental data have been analyzed following the procedure that is detailed elsewhere [29]. From several open-aperture curves the nonlinear absorption parameter (β) and the imaginary part of the third order nonlinear susceptibility (Im$\chi^{(3)}$) have been obtained as shown in Table 1. Additionally, the valley-peak transmission difference of the divided Z-scans allowed the determination of the nonlinear refractive parameter (γ'), the nonlinear refractive index (n_2), and the real part of the third order nonlinear susceptibility (Re$\chi^{(3)}$) (see Table 1). While there is considerable literature on the use of Fe:ZnS for mid-IR lasing, related materials in crystal form, are reported for saturable absorber applications [14, 15, 42].

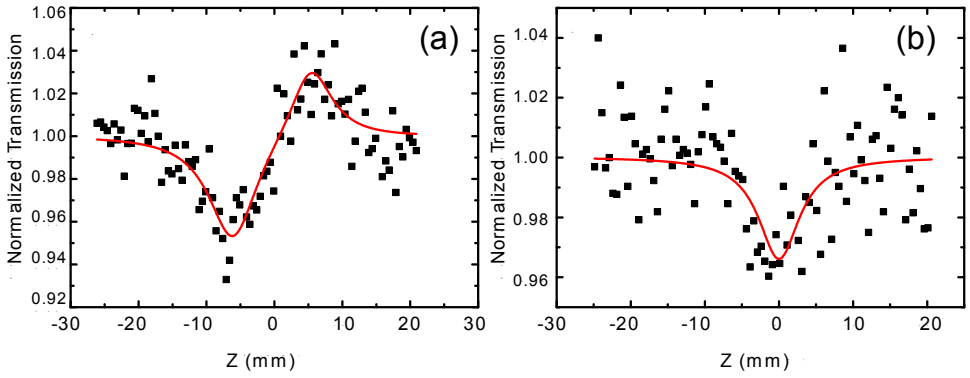

Fig. 4. Nonlinear transmission of the 5.8% Fe doped film measured at 532 nm. (a) Divided scan, and (b) an open-aperture scan.

Optical Materials EXPRESS

Table 1. Nonlinear parameters for Fe:ZnS films at 532 nm.

β $(\times 10^{-7} m/W)$	$Im\chi^{(3)}$ $(\times 10^{-8} esu)$	γ' $(\times 10^{-13} m^2/W)$	n_2 $(\times 10^{-6} esu)$	$\mathrm{Re}\chi^{(3)}$ $(\times 10^{-8} esu)$	$\chi^{(3)}$ $(\times 10^{-8} esu)$
6.7	1.0	2.1	1.2	7.8	7.9

The experimental findings show high nonlinear refraction and nonlinear absorption parameters. By comparing the real and imaginary part of the third order nonlinear susceptibility it can be seen that the real part is about 8 times higher indicating that the nonlinear refraction dominates the nonlinear optical response. These findings illustrate the significant optical nonlinearities of the Fe:ZnS thin films, which can be utilized in a variety of applications such as optical switching and optical limiting. The effects of the Fe content on the nonlinear refraction and absorption merit further study - for example, shorter pulse widths will allow the elimination of thermal effects, which may play a role in some of the current findings. The laser irradiation parameters can be chosen to tune the nonlinearities for specific applications, with the selected excitation wavelength anticipated to have a significant impact.

3.5. Transmission electron microscopy

High resolution transmission electron microscopy allows direct determination of the crystal structure, and electron diffraction can differentiate cubic "zinc blende" (ZB) from wurtzite (W) material, allowing a detailed determination of the structure of the films, at the atomic level, to be made. Scanning TEM (STEM) images shown in Fig. 5 (a)-(c) of film surfaces with 0, 1.2 and 7.5 at.% Fe demonstrate that the lateral sizes of the crystalline grains decrease upon the addition of Fe to the films. Bright field TEM images shown in Fig. 5 (d)-(f) reveal that the films are comprised of nanoscale columns. Each of the nanocolumns run through the entire film

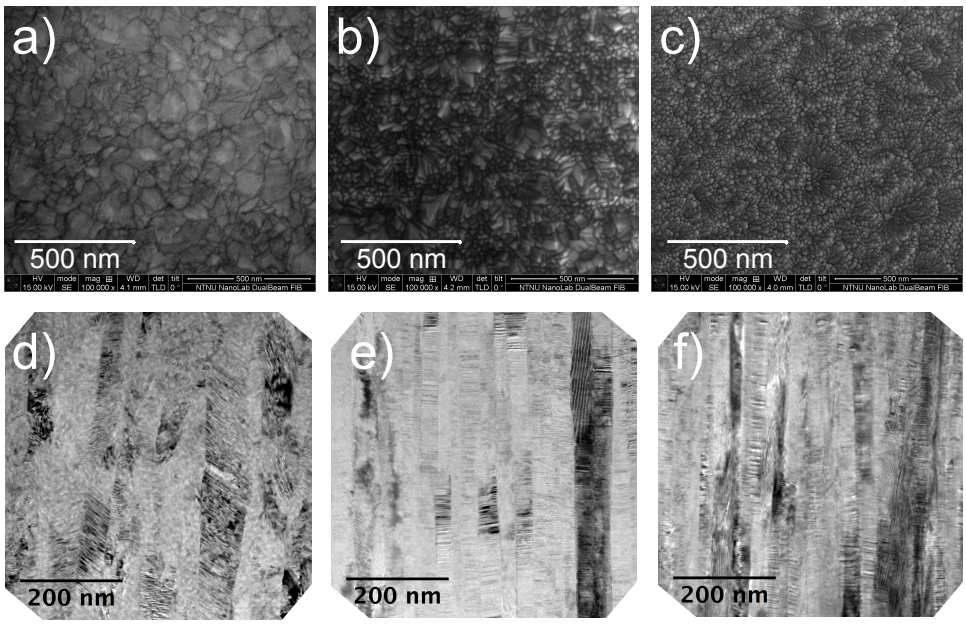

Fig. 5. Electron microscopy images. Top row, STEM of the surfaces of films with a) 0 b)1.2 and c)7.5% Fe, and bottom row, cross-sectional bright field TEM images for d) 0 e)1.2 and f)7.5% Fe

Optical Materials EXPRESS

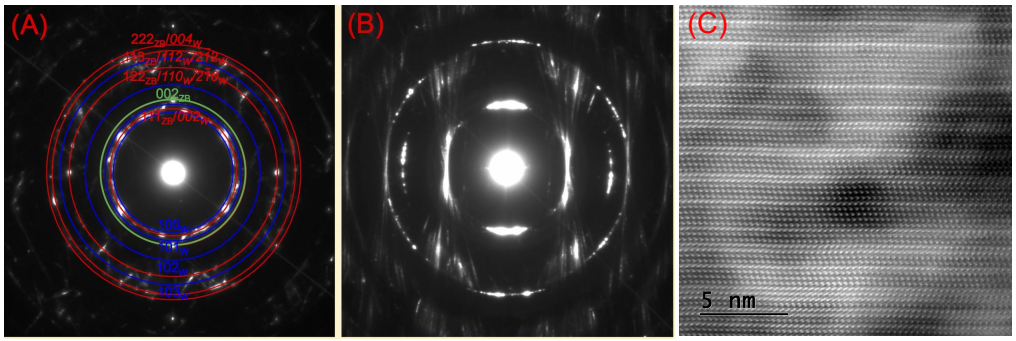

Fig. 6. (a) Electron diffraction pattern of the undoped ZnS. Red circles indicate positions of Bragg reflections that can be either ZB or W, the green circle indicates the unique (002) ZB reflections, and the blue circles indicate possible positions of the unique W reflections. (b) 7.5 at.% Fe:ZnS electron diffraction pattern. (c) High-angle annular dark-field imaging STEM showing extreme twinning along a nanocolumn in the sample.

thickness, but the lateral dimension decreases with increasing Fe doping, possibly due to an enhanced sticking coefficient for the ZnS during nucleation of the grains. Electron diffraction results (Fig. 6 (a)) show that the undoped ZnS film has a random mixture of cubic ZB and hexagonal W crystal structure with no preferred crystalline texture.

The Fe doped films (Fig. 6 (b)) have a pure ZB crystal structure with a strong preferred texture where the [111] ZB direction tends to align perpendicular to the plane of the substrate. High angle annular dark field (HAADF) STEM cross-sectional images of the doped samples (see Fig. 6 (c)) show that each of the nanocolumns is heavily twinned by (111) walls and with twin domains thicknesses ranging from a single monolayer up to a few tens of unit cells. These results demonstrate that even large Fe doping into ZnS caused little crystalline disruption aside from the appearance of extreme twin defect densities. (It should be noted that twin defects are also common in pure ZnS crystals). The primary disorder observed is the increase in the number of grain boundaries; the material within the columns for even the highest concentration films studied had few, if any defects other than twins. No evidence of Fe clusters was observed.

3.6. XRD

The XRD data of the Fe doped samples on Si (100) substrates with collection angles of15–85° is shown in Fig. 7. Two main peaks around 28.5° and 59.0° were observed and following TEM analysis were attributed to cubic (111) and (222) reflections. The intensity of the (222) peak was low and only (111) reflection was used in the analysis.

As can be seen in Fig. 7 (a), the pure ZnS film grown at the RT showed the lowest intensity peak, which is expected for a low temperature growth due to loss of any preferred texture. The Fe doping resulted in an increase of the signal by more than two orders of magnitudes (indicative of a preferred crystalline texture, with the [111] direction perpendicular to the film. This change in preferred texture is identical to the TEM observations. The Fe doping also correlates with a shift in the position of the peaks, as shown in Fig. 7 (b). These shifts can be a result of a slight reduction in the lattice constant due to the smaller ionic radius of Fe and a presence of the defects in the crystal structure. The observed shifting of the main diffraction peaks suggests the decrease of the unit cell and, therefore, substitutional incorporation of Fe, which is in the agreement with Raman data. The mean grain size calculated by the Scherrer formula [43] was found to be around 65 nm independent of the Fe concentration, but stress and substitutional effects are known to influence these results.

Optical Materials EXPRESS

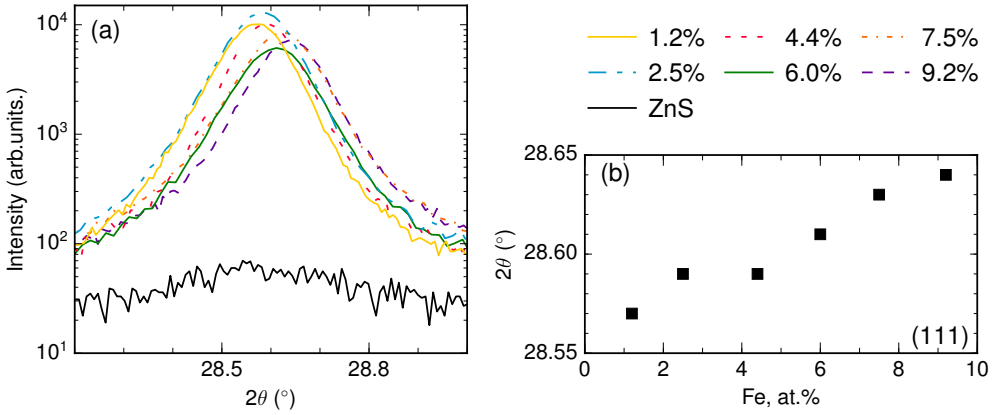

Fig. 7. XRD spectra of samples with different amount of Fe grown on Si (100) substrate. (a) Increased intensity of the (111) reflection after doping with Fe compared with undoped ZnS. (b) Positions of the (111) reflection in Fe:ZnS samples.

4. Conclusion

In conclusion, we have demonstrated that Fe-doped ZnS films vapor deposited onto room temperature substrates exhibit substitutional incorporation of the Fe up to 4 at.% without excessive disruption of the underlying crystal structure. The iron-induced absorption peak around 2.8 µm remains well-isolated for these concentrations. Undoped ZnS films have a random mixture of cubic zincblende and hexagonal wurtzite crystal structures, while in contrast, the Fe-doped films have a pure zincblende crystal structure with a strongly preferred (111) texture and a high density of twin defects. Raman and TEM analyses confirm substitutional incorporation of Fe in these cubic ZnS films at low concentrations. Visible absorption and the Optical Kerr Effect increase significantly for films with higher Fe content, but the spectral shape of the iron-related infrared absorption is unchanged. Nonlinear optical behavior is observed at 532, 795 and 2940 nm, with saturable absorption of the Fe-induced levels confirmed for Fe concentrations both above and below 4 at .%. The Z-scans determine the real and the imaginary part of the third order nonlinear susceptibility, which is challenging with the OKE technique. The fact that two-photon absorption will promote carriers above the gap for the Z-scan measurements is most likely responsible for the difference in the observed $\chi^{(3)}$. These results demonstrate that vapor deposited films of Fe-doped ZnS have potential non-linear applications in mid-infrared systems.

Funding

Norwegian University for Science and Technology; Norges Forskningsråd (219686/O70, 221675, and 262232/O70).

Acknowledgments

We acknowledge laboratory support by Erik Nikolai Lysne.